HPU/TiO$_2$ nanoparticles decorated RGO nanocomposite as a smart material with sunlight-induced self-cleaning attribute

Highlights

This chapter demonstrates the fabrication, characterization and property evaluation of HPU/TiO$_2$ nanoparticles decorated-reduced graphene oxide (HPU/TiO$_2$-RGO) nanocomposite to achieve a combined attributes of shape memory, self-healing and photo-induced self-cleaning properties in a single material. The fabricated nanocomposite exhibited composition and dose-dependent mechanical properties with excellent shape recovery ratio (92–95%) as well as shape recovery rate (1-5 min) under exposure to sunlight. Most importantly, the nanocomposite demonstrated both repeatable intrinsic self-healing (within 7.5–10 min) and efficient self-cleaning ability by removing model dirt, methylene blue, (within 2–3 h) under the same energy exposure. The study also showed that these novel properties of the nanocomposite can be tuned by judicious choice of amount and composition of the TiO$_2$-RGO nanohybrid. The presence of an adequate amount of RGO (0.5–1 wt%) in the nanocomposite helps in rapid and efficient healing, whereas a relatively high amount of TiO$_2$ nanoparticles (5–10 wt%) aids in achieving good self-cleaning properties. Therefore, the nanocomposite could be a promising futuristic material for many advanced applications.

6.1. Introduction

Smart polymers are carved a distinct niche in materials science over the last few decades.[1,2] Such polymers can respond to a stimulus as desired.[3] SMP is one of the smart polymers which can return from a deformed state (temporary shape) to their original state (permanent shape) upon triggering by a suitable external stimulus as mentioned in sub-chapter 3B, section 3.B.1.[4] The design and development of SHP and self-cleaning polymers (SCP) are also attracted significant interest over the past decades as such polymers reduce energy consumption and minimize use of resource and generation of waste.[5,6] SHPs are also a class of smart polymers like SMP. SHP possesses the ability to repair the damage caused by mechanical strain over time, whereas SCPs are a special class of polymers that keep the surface free from dirt and grime as discussed in Chapter 1, section 1.6.[7,8]

A lot of polymeric materials are developed which exhibit SME, self-healing and self-cleaning properties.[9-16] But it is highly challenging to endow the combined properties in a single material. The structural incompatibility among such types of polymers is one of the crucial reasons for this difficulty. In SMP, a permanent network structure is essential to restrict the chain motion. Thus, such polymers are usually stiff and possess a high modulus along with flexible soft segment.[17] These structural features of SMP are contradictory to those of SHP where high chain mobility and interdiffusion are essential.[18] Again, either a photocatalytic material or a superhydrophobic/superhydrophilic surface is required in SCP for the removal of dirt.[8,19] Therefore, tuning these properties in a single polymeric material is of fundamental and applied interest of material scientists in recent time. In this context, RGO based HPU nanocomposites are demonstrated excellent SME and repeatable healing ability under the exposure to MW and sunlight as stated in the previous chapters.

In this context, semiconductor photocatalyst (SP), such as TiO₂, are widely used for photodegradation of organic compounds, especially for decontamination of air and water and hence they are found to be exciting materials for achieving photoinduced self-cleaning polymeric materials.[8] The self-cleaning properties of TiO₂ originate from the photocatalytic oxidative decomposition of organic contaminants.[20] However, pure TiO₂ is activated by only UV light and the generated electron–hole pairs that demonstrate a high rate of recombination. Hence, this hampers its practical applicability.[21] Numerous approaches are attempted to develop such photocatalyst and the improvement in the efficiency is achieved by dye sensitization and doping with various metal ions as well as some special nonmetals such as nitrogen, carbon and sulfur. Thus, various carbonaceous materials such as activated

carbons, carbon nanotubes and graphene based SP nanohybrids are widely used for photodegradation of contaminants with improved photocatalytic performance.[21] In this vein, a TiO_2/reduced graphene oxide nanohybrid (TiO_2-RGO) exhibited improved photocatalytic activity under visible light or sunlight.[22,23]

Therefore, an attempt was made to achieve combined attributes of shape memory, self-healing and self-cleaning properties in HPU nanocomposites using different wt% of the TiO_2-RGO nanohybrid at variable compositions. Also, the effect of composition and loading of the nanohybrid on tuning the self-healing and self-cleaning properties of the nanocomposite was investigated.

6.2. Experimental

6.2.1. Materials

The same monoglyceride of the castor oil, TDI, PCL and BD as described in Chapter 2, section 2.2.1were used for the preparation of HPU nanocomposite. The same GO and *C. esculenta* leaf extract as reported in sub-chapter 3A were used for the preparation of TiO_2-RGO nanohybrid.

TiO_2 nanoparticles were procured from Sigma Aldrich, India. TiO_2 nanoparticles are widely used as UV-resistant material and in the field of producing chemical fiber, printing ink, self-cleaning materials, antibacterial material, air purification, cosmetics, sunscreen cream, etc. Here, the nanoparticles were used to prepare the nanohybrid.

6.2.2. Characterization

FTIR, XRD, DSC and TGA analyses, and mechanical tests were performed under the same conditions and by using the same instruments as described in Chapter 2, section 2.2.2. Raman spectra of TiO_2-RGO nanohybrids were taken by same Raman spectroscope and same condition as mentioned in sub-chapter 3A, section 3A.2.2. The morphology and SAED pattern of the nanohybrid and the nanocomposite were analyzed by same HRTEM as mentioned in sub-chapter 3A, section 3A.2.2. Shape memory test under sunlight was performed as mentioned in the sub-chapter 3C, section 3C.2.2. Self-healing test was carried out under sunlight as mentioned in Chapter 4, section 4.2.2. A thermocouple (Metravi, 305XL) was used to measure the surface temperature of the sample during self-healing and shape memory tests. The self-cleaning properties of the nanocomposite were evaluated by photocatalytic degradation of methylene blue (MB) as a model compound. In the typical

test, the nanocomposite film (average weight 0.8–1.0 g) was chopped in to small pieces (dimensions almost 5×5 mm^2) and these chopped polymer films were immersed in 50 mL of MB solution (60 ppm). Then the solution was kept in the dark for 1 h to obtain equilibrium. Afterward, the solution was exposed to sunlight (sunny day, average temperature: 38 ± 1 °C, humidity: $62 \pm 1\%$, and light intensity: 90,000–1,00,000 lux) for photodegradation of the dye. The concentration change of MB was monitored by measuring the UV absorbance intensity at 664 nm at particular irradiation time intervals.

6.2.3. Preparation of TiO$_2$-RGO nanohybrid

To prepare the nanohybrid, required amount of GO and TiO$_2$ nanoparticles were taken in a water/ethanol (50:50 v/v) system. Then, the mixture was stirred for 1 h and ultrasonicated for 10 min to obtain a homogenous dispersion of GO and TiO$_2$ nanoparticles. Then *C. esculenta* leaf extract (10 mL) was added to the homogeneous dispersion (50 mL) present in a single necked round bottomed flask and stirred for 5 h at room temperature to reduce GO. Three different nanohybrids were prepared using different weight ratios of TiO$_2$ and RGO (1:1, 5:1 and 10:1) and they were coded as T$_1$RGO, T$_5$RGO and T$_{10}$RGO respectively.

### 6.2.4. Preparation of HPU/TiO$_2$-RGO nanocomposite

HPU/TiO$_2$-RGO nanocomposite was prepared following the same method which was used to prepare HPU/RGO nanocomposite in the sub-chapter 3C, section 3C.2.4. Only required amounts of dispersed TiO$_2$-RGO nanohybrid in DMAc (different wt%: 0.5, 1 and 2 with respect to total weight of nanocomposite) were incorporated instead of RGO in 1st step of the polymerization reaction to obtain *in situ* HPU/TiO$_2$-RGO nanocomposite. HPU/TiO$_2$-RGO nanocomposites were prepared using different wt% of the three nanohybrids separately (T$_1$RGO, T$_5$RGO and T$_{10}$RGO). The nanocomposites were encoded as HPU/T$_x$RGO$_y$ where the digits *x* and *y* imply the contents of TiO$_2$ in the nanohybrid and nanohybrid in the nanocomposite respectively.

6.3. Results and discussion

6.3.1. Characterization of TiO$_2$-RGO nanohybrid

Reduction of GO and formation of the nanohybrid were analyzed by a FTIR spectroscopic technique. FTIR spectra of GO-TiO$_2$ and the T$_{10}$RGO nanohybrid are shown in **Figure 6.1**. After the reduction of GO, the decreased in broadening of the OH stretching band at 3410

cm^{-1} and the disappearance of the C=O band at 1720 cm^{-1} indicate that the oxygenated groups of GO are reduced in the nanohybrid. Also, the presence of the Ti–O stretching vibration band at 660 cm^{-1} indicates the presence of TiO_2 nanoparticles in the nanohybrid.[24]
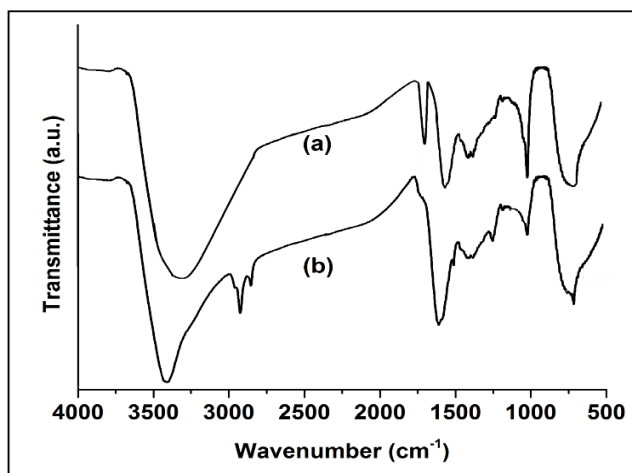
**Figure 6.1** FTIR spectra of (a) GO-TiO_2 and (b) $T_{10}RGO$

Raman spectroscopy is one of the most valuable techniques to analyze the ordered/disordered structures of carbonaceous and titanium oxide-based materials.[25,26] **Figure 6.2** shows the Raman spectra of GO and $T_{10}RGO$. The intensity ratio of I_D/I_G increased from 0.88 to 1.09 which can be attributed to more defects/disorders in graphitized structures in the nanohybrid.[27] The appearance of the 2D peak in the Raman spectra of GO and the nanohybrid at ~2690 cm^{-1} indicates the presence of multilayer graphene sheets in GO and the nanohybrid.[27] Also, the peak at 635 cm^{-1} in the Raman spectra of the nanohybrid is assigned to the presence of anatase TiO_2.[28]
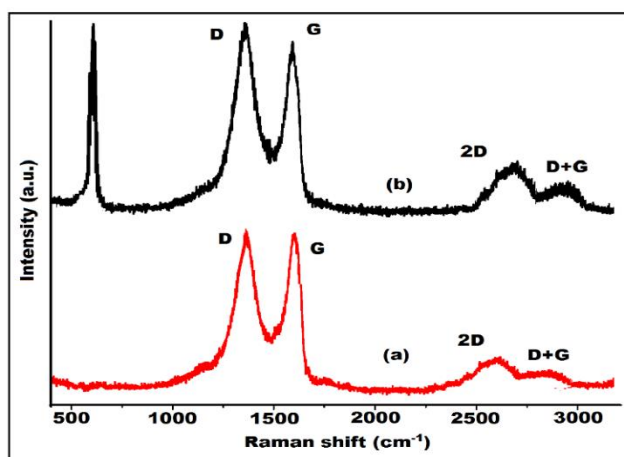
**Figure 6.2** Raman spectra of (a) GO and (b) $T_{10}RGO$

The XRD patterns of pure TiO_2 nanoparticles and the nanohybrid are shown in **Figure 6.3**. The peaks of 2θ values at 25.3, 37.9, 48.0, 54.4, 56.6, and 62.8° are assigned to the (101), (004), (200), (105), (211) and (204) planes of anatase TiO_2, respectively.[29] It should be noted that there is no separate peak found for RGO in the nanohybrid. This may be due to the presence of less crystalline RGO than TiO_2. Moreover, the characteristic peak of RGO at around 26° may be masked by the main peak of anatase TiO_2 at 25.3°.[30]
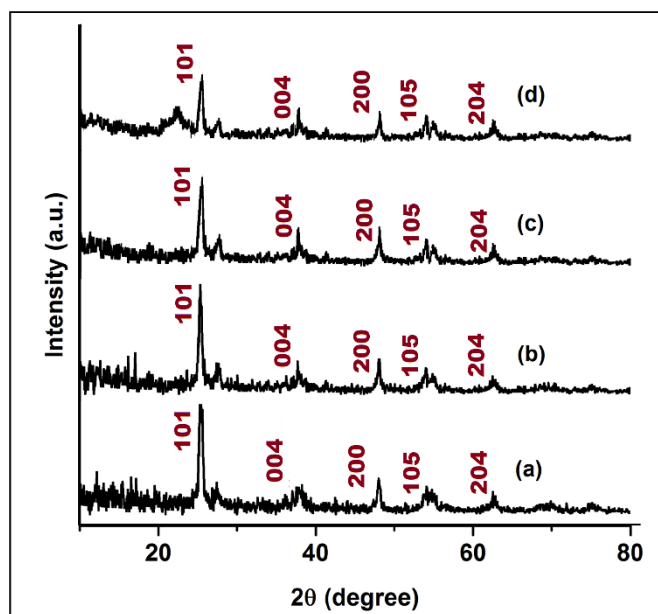

Figure 6.3 XRD patterns of (a) TiO_2 nanoparticles, (b) $T_{10}RGO$, (c) T_5RGO and (d) T_1RGO

TGA thermograms of pure TiO_2 nanoparticles and the nanohybrids showed a marginal weight loss in **Figure 6.4**. It is clear from **Figure 6.4** that the amount of weight loss increased with increasing amounts of RGO content in the nanohybrid. As RGO contains some amount of oxygenated groups which are degraded at higher temperature. In addition to that the ring carbon of RGO also burned at higher temperature as mentioned in sub-chapter 3A, section 3A.3.7. The weight loss of TiO_2 nanoparticle is ascribed to the loss of the adsorbed H_2O and the crystallization of amorphous TiO_2 into anatase TiO_2.[31]

HRTEM image of the nanohybrid demonstrates that TiO_2 nanoparticles are well-dispersed on the surface of the RGO sheet (**Figure 6.5**a). **Figure 6.5**b shows that the crystal lattice fringes with a d-spacing of 0.35 nm corresponding to the (101) plane of anatase TiO_2.[32] This suggests that TiO_2 nanoparticles have a well-ordered structure and a high degree of crystallinity.
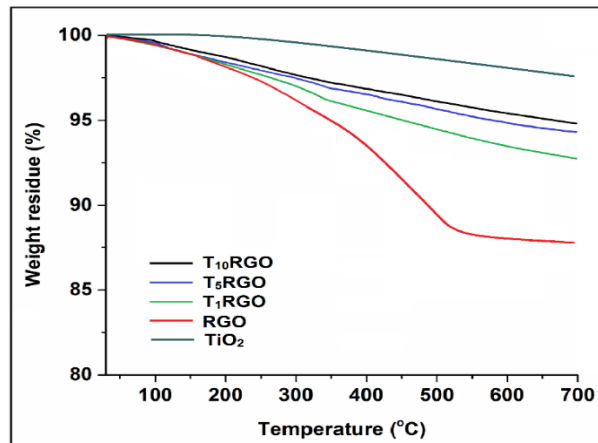
Figure 6.4 TGA thermograms of the TiO$_2$ nanoparticles, RGO and TiO$_2$–RGO nanohybrids
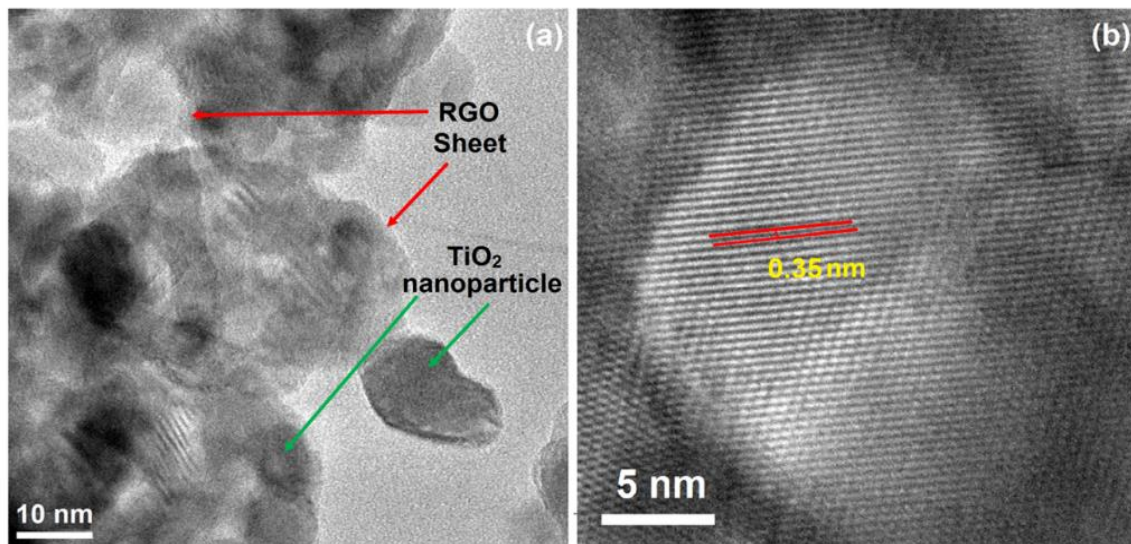
Figure 6.5 HRTEM images of the T$_1$RGO nanohybrid (a) at low resolution showing the presence of RGO and TiO$_2$ nanoparticles and (b) at high resolution showing crystal lattice fringes of TiO$_2$ nanoparticles

6.3.2. Mechanical properties of HPU/TiO$_2$-RGO nanocomposite

The effect of the nanohybrid on the mechanical properties of the nanocomposite was observed as functions of its loading and composition (**Table 6.1**). After incorporation of the nanohybrid, the mechanical properties such as the tensile strength, tensile modulus, toughness and elongation at break for all the nanocomposites significantly improved over the pristine HPU (**Table 6.1**). This is attributed to the good dispersion of the nanohybrid, good compatibility and significant interfacial interactions between HPU and the nanohybrid.[33,34] The nanohybrid contains sufficient polar hydroxyl groups and polar Ti–O

groups. These groups can form covalent and noncovalent bonds with HPU chains as the nanohybrid was incorporated in the 1st step of the polymerization similar to HPU/RGO nanocomposite as stated in sub-chapter 3C, section 3C.3.4. Thus the hard segments of HPU are stiffened, improving the mechanical properties of HPU nanocomposites.[35] The mechanical properties of the nanocomposites were found to be highly dependent on the composition of the nanohybrid and its loading. The nanocomposite with the T_1RGO nanohybrid exhibited superior mechanical properties to nanocomposites with T_5RGO and T_{10}RGO nanohybrids. As RGO possesses a higher aspect ratio than that of TiO$_2$ nanoparticles, the mechanical properties of the nanohybrid are improved to a greater extent with the amount of RGO present in it.[25] Also, a high amount of nanohybrid deteriorated the mechanical properties which may be due to the agglomeration of the nanohybrid and irregular load transfer from HPU chains to the nanohybrid. It is most interesting to note that HPU/T_1RGO1 and HPU/T_{10}RGO5 contain almost the same amount of RGO, but their mechanical properties are drastically different. This may be due to the presence of a high amount of TiO$_2$ nanoparticles which retard the interaction of RGO with HPU chains in the HPU/T_{10}RGO10 nanocomposite. In addition, all the nanocomposites showed higher elongation at break than pristine HPU. This is due to the presence of RGO in the nanohybrid which is an elasto-plastic material.[36]

Table 6.1 Mechanical properties of HPU/TiO$_2$-RGO nanocomposite

Nanocomposite	Tensile strength (MPa)	Tensile modulus (MPa)	Toughness (MJm^{-3})	Elongation at break (%)
HPU/T_1RGO1	23.4 ± 0.5	21.4 ± 1.8	128.7 ± 6.7	1245 ± 41
HPU/T_1RGO2	25.7 ± 0.6	23.7 ± 2.1	141.6 ± 8.2	1320 ± 35
HPU/T_5RGO1	20.3 ± 0.4	18.6 ± 1.4	102.1 ± 3.4	1043 ± 22
HPU/T_5RGO2	21.8 ± 0.2	19.8 ± 1.2	110.6 ± 4.4	1124 ± 25
HPU/T_{10}RGO1	17.3 ± 0.2	15.9 ± 0.9	88.4 ± 2.7	910 ± 15
HPU/T_{10}RGO2	18.2 ± 0.3	16.3 ± 1.1	95.3 ± 3.1	987 ± 26
HPU/T_{10}RGO5	16.1 ± 0.3	14.1 ± 1.2	78.4 ± 3.3	1035 ± 32
HPU/T_{10}RGO10	15.3 ± 0.4	12.5 ± 0.7	69.6 ± 2.3	1095 ± 35

### 6.3.3. Thermal properties of HPU/TiO$_2$-RGO nanocomposite

DSC curves of HPU/TiO$_2$-RGO nanocomposites are shown in **Figure 6.6**. It is seen that T$_m$ of the soft segment was considerably dependent on the amount of nanohybrid and T$_m$ was shifted to higher temperature with the increase of the nanohybrid content. Here, it is important to notice that T$_m$ minutely changed with compositional variation of the nanohybrid but was highly dependent on the loading of the nanohybrid. As the nanohybrid serves as a nucleating agent as mentioned in sub-chapter 3C, section 3C.3.5, the crystallinity of the nanocomposite enhanced with the nanohybrid content.[37] Also, T$_m$ of the nanocomposites shifted to a higher temperature due to the presence of a higher number of interactions between the nanohybrid and HPU chains with increase in the amount of TiO$_2$-RGO nanohybrid in the nanocomposite.
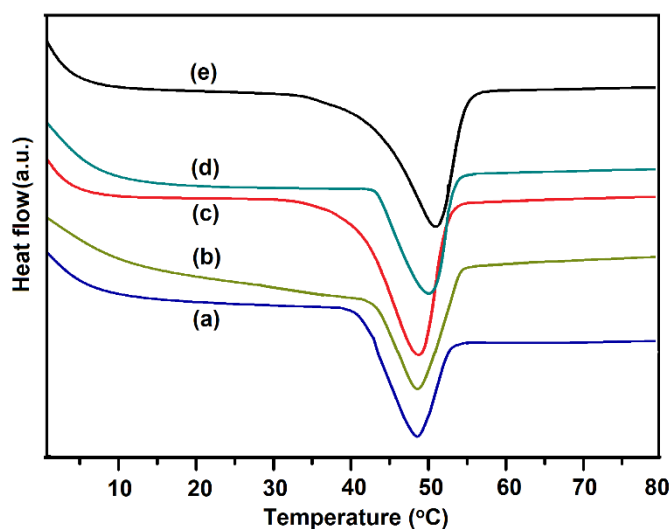
Figure 6.6 DSC curves of (a) HPU/T$_1$RGO1, (b) HPU/T$_5$RGO1, (c) HPU/T$_{10}$RGO1, (d) HPU/T$_{10}$RGO5 and (e) HPU/T$_{10}$RGO10

The thermal behaviors of HPU/TiO$_2$-RGO nanocomposites were studied using TGA, as shown in **Figure 6.7**. All the thermograms demonstrated two step degradation profiles for the presence of soft and hard segments in HPU.[17] These suggest that the nature and loading of the nanohybrid do not significantly influence the degradation mechanism of the nanocomposite. The initial degradation temperature of the nanocomposite shifted to a notably higher temperature with the nanohybrid content. The barrier properties of the nanohybrid are mainly responsible for improving the thermal stabilization of the nanocomposite. Also, the presence of an inorganic component provides additional heat insulating capacity, which stabilizes the nanocomposite against thermal decomposition.

Moreover, the presence of strong covalent and non-covalent interactions between the nanohybrid and HPU matrix enhances the thermal stability of the nanocomposites.
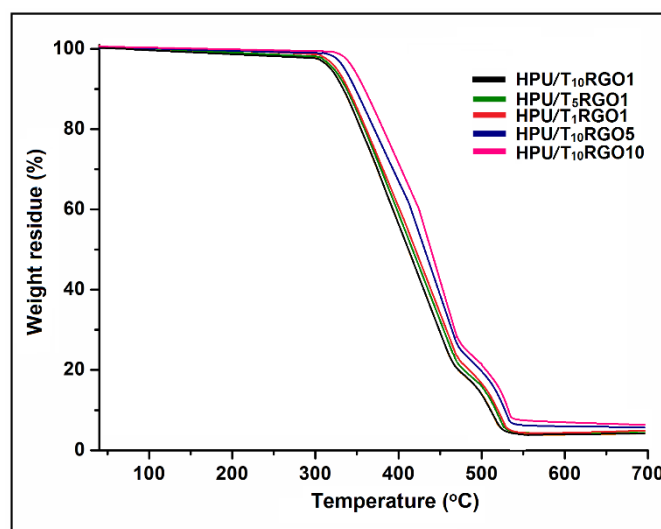
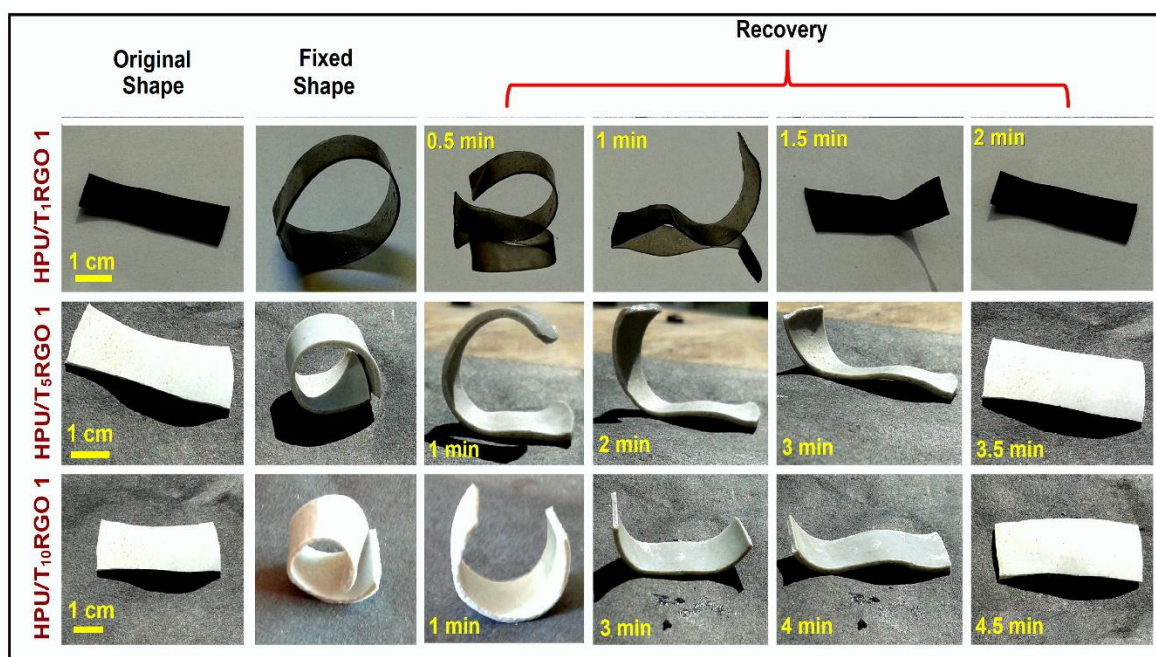**Figure 6.7** TGA thermograms of HPU/TiO$_2$-RGO nanocomposite

6.3.4. Shape memory behavior of HPU/TiO$_2$-RGO nanocomposite

The sunlight induced SME was measured for HPU/TiO$_2$-RGO nanocomposites. Shape recovery and shape fixity values are tabulated in **Table 6.2**. All the nanocomposites exhibited an excellent SME (**Figure 6.8**). The nanocomposite showed rapid shape recovery compared to pristine HPU due to the presence of the nanohybrid that possesses high sunlight absorbing capacity, especially RGO as mentioned in sub-chapter 3C, section 3C.3.7.[38] The effect of composition and loading of the nanohybrid on shape memory behavior was also investigated. In particular, the shape recovery time decreased significantly when the amount of RGO is high in the nanohybrid, so the T$_1$RGO based nanocomposite exhibited the highest SME. The rapid shape recovery rate of the T$_1$RGO-incorporated nanocomposite is attributed to the sunlight absorbing ability of the nanohybrid. Here, sunlight was used as the energy source. Shape recovery is achieved by physical changes unlike the other light induced shape memory effects where some chemical reactions generally take place such as photo-crosslinking, photo-cleavage reaction, etc.

As RGO is a conducting material, it absorbs the energy from sunlight and efficiently transfers the absorbed energy to the HPU matrix. Therefore, the nanocomposite reaches its transition temperature easily to recover its shape.

**Table 6.2** Shape memory behavior of HPU/TiO$_2$-RGO nanocomposite

Nanocomposite	Shape recovery ratio (%)	Shape recovery time (min)	Shape fixity (%)
HPU/T$_1$RGO1	97.8 ± 0.2	2.03 ± 0.04	92.5 ± 0.1
HPU/T$_1$RGO2	98.4 ± 0.3	1.48 ± 0.02	92.1 ± 0.2
HPU/T$_5$RGO1	96.8 ± 0.2	3.44 ± 0.06	94.3 ± 0.2
HPU/T$_5$RGO2	97.2 ± 0.1	3.03 ± 0.02	92.8 ± 0.1
HPU/T$_{10}$RGO1	96.2 ± 0.2	4.52 ± 0.06	94.1 ± 0.2
HPU/T$_{10}$RGO2	96.6 ± 0.2	4.06 ± 0.04	94.2 ± 0.1
HPU/T$_{10}$RGO5	97.3 ± 0.1	5.03 ± 0.02	93.2 ± 0.2
HPU/T$_{10}$RGO10	94.3 ± 0.1	5.56 ± 0.04	95.3 ± 0.1

Figure 6.8 Series of digital photographs showing the shape memory behavior of HPU/TiO$_2$-RGO nanocomposite under exposure to sunlight

6.3.5. Self-healing properties of HPU/TiO$_2$-RGO nanocomposite

A crack in the nanocomposite was effectively healed by the exposure to sunlight as shown in **Figure 6.9**. The healing efficiency of the nanocomposite strongly depends on loading and the nature of the nanohybrid. Here, it is pertinent to mention that HPU nanocomposites with

T$_5$RGO and T$_{10}$RGO nanohybrids did not show any healing effect upon exposure to sunlight even after a long time. HPU/T$_1$RGO nanocomposites with different loadings were only effectively healed within 7.5–10 min under direct sunlight (**Figure 6.9**a).
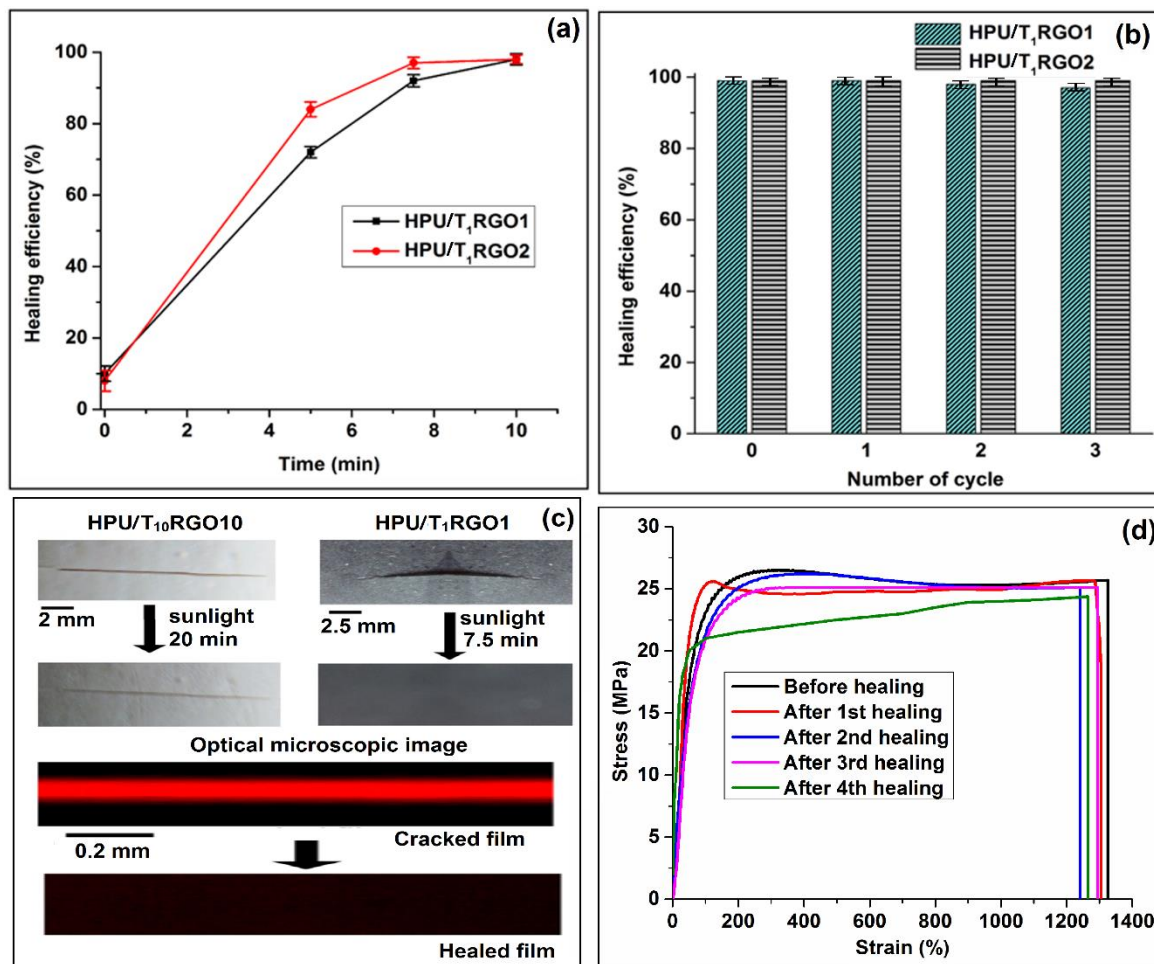
Figure 6.9 (a) Healing efficiency of the nanocomposite under sunlight, (b) repeatable healing efficiency of the nanocomposite, (c) digital and optical microscopic photographs of cracked and healed nanocomposite films and (d) representative stress–strain profiles of HPU/T$_1$RGO2, before and after healing with different repeating cycles

It is well-known that the SME assists in the healing process by bringing the polymeric chains in proximity to the crack as mentioned in Chapter 4, section 4.3.8.[39] Indeed, all the nanocomposites exhibited a SME though only HPU/T$_1$RGO nanocomposites showed self-healing ability. Both SMP and SHP require rearrangement of polymeric chains but a huge amount of energy is required to soften and interdiffuse the soft segment chains of HPU in the fracture place to heal it as mention in Chapter 4, section 4.3.8.

The surface temperature of the sample was found to be in the range of 44.5 to 45.8 °C at the time of healing. Whereas, comparatively less energy is needed to rearrange the orientation of polymeric chains to achieve the original shape of SMPs.[40] This tunable healing property mainly comes from appropriate variation of the composition of the nanohybrid. From the results, it is clear that a high amount of RGO is responsible for self-healing as it is a good sunlight absorber as mentioned in sub-chapter 3C, section 3C.3.7. Therefore, the HPU/T$_1$RGO nanocomposite exhibited good healing capability even at a low dose level (1 wt%). HPU/T$_5$RGO and HPU/T$_{10}$RGO nanocomposites containing 1 or 2 wt% of the nanohybrid did not exhibit a healing effect. This may be due to the presence of a low amount of RGO in the nanocomposites and also the surface of RGO is covered by TiO$_2$ nanoparticles in the T$_5$RGO and T$_{10}$RGO nanohybrids. Therefore, they are unable to absorb sufficient energy for polymeric chain diffusion. Although, the HPU/T$_{10}$RGO10 nanocomposite contains a sufficient amount of RGO in the system (the same amount of RGO as that present in the HPU/T$_1$RGO1 nanocomposite which showed good healing efficiency), but this nanocomposite did not demonstrate any healing ability. This may be due to the agglomeration of the nanohybrid. As a result, the nanohybrid is not uniformly distributed in the nanocomposite which prevents the efficient transfer of energy to the soft segment of HPU. Also, the T$_{10}$RGO nanohybrid contains a high amount of TiO$_2$ nanoparticles which cover the effective surface area of RGO. Therefore, the nanohybrid also absorbs a low amount of sunlight. During the healing process, T$_1$RGO absorbed energy from sunlight and then transferred the energy to the soft segment of the HPU matrix. This transferred energy aids in softening the segment and the segment starts molecular diffusion towards the crack to repair it. Meanwhile, the hard segment of HPU helps to retain its dimension. Appropriate variation of the composition of the nanohybrid plays a vital role in achieving the desired self-healing ability.

Similar to previous work (Chapter 5), the HPU/T$_1$RGO nanocomposite also showed repeated healing as it is achieved by the interdiffusion of soft segments of HPU. Thus, even after the third cycle of experiment, the healing ability of the nanocomposite remains almost the same (**Figure 6.9**b). Representative stress–strain curves for before and after healing with different repeating cycles are shown in **Figure 6.9**d.

6.3.6. Sunlight induced self-cleaning properties of HPU/TiO$_2$-RGO nanocomposite

In this study, MB was chosen as model dirt for testing sunlight induced self-cleaning properties of the prepared nanocomposites. Photocatalytic degradation of the dye was

investigated using chopped pieces of HPU/TiO$_2$-RGO nanocomposite film under exposure of sunlight. The degradation of aqueous MB solution based on its concentration changes with time is shown in **Figure 6.10**.
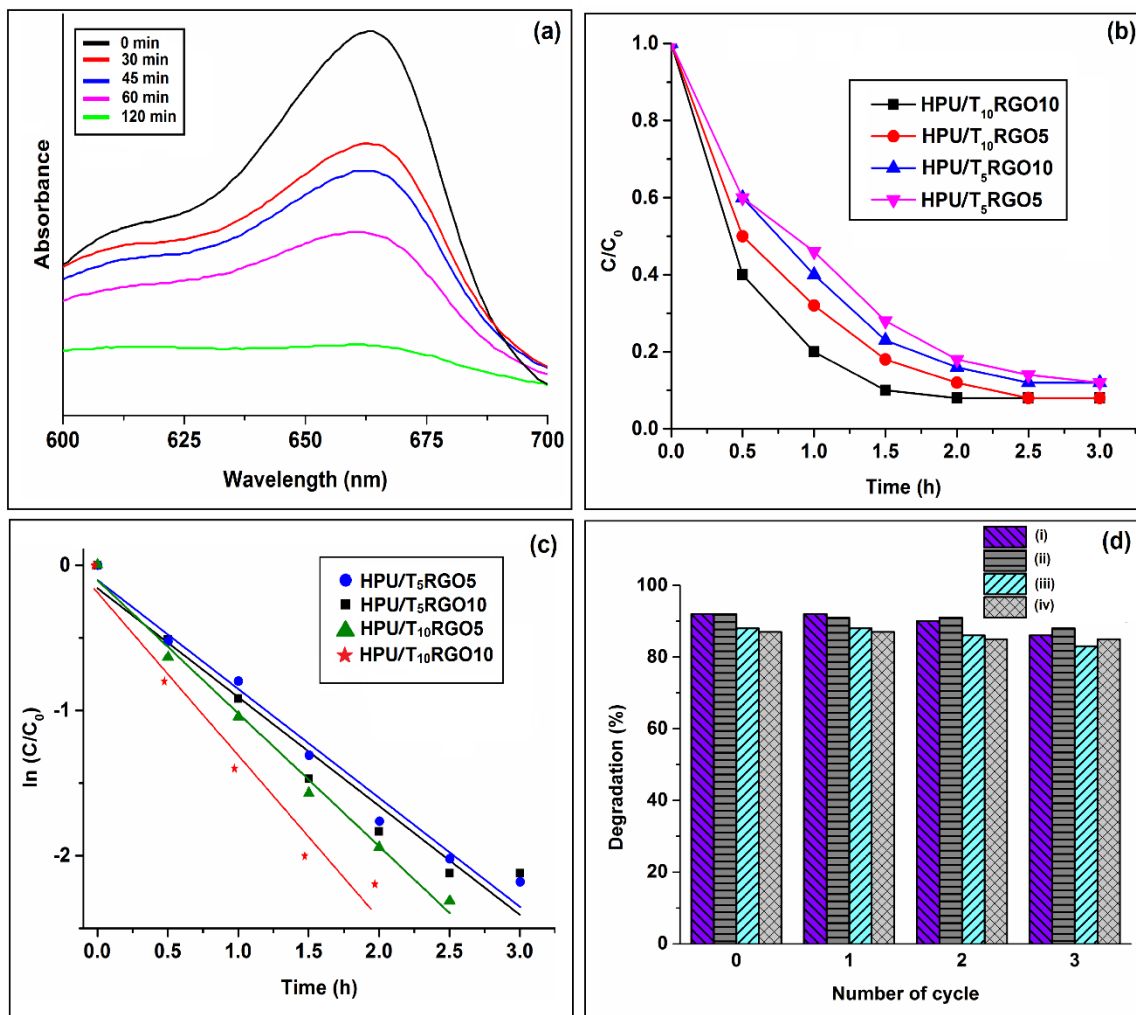

Figure 6.10 (a) Time-dependent UV absorption spectra of MB solutions during sunlight irradiation, (b) degradation curves of the MB by the nanocomposite, (c) degradation kinetic curve fitting for the pseudo-first order model and (d) repeatable photocatalytic efficiency of (i) HPU/T$_{10}$RGO10, (ii) HPU/T$_{10}$RGO5, (iii) HPU/T$_5$RGO10 and (iv) HPU/T$_5$RGO5

Pure TiO$_2$ nanoparticles can degrade the dye but their efficiency is very poor due to the high recombination rate of generated hole/electron (h$^+$/e$^-$) pairs as mentioned earlier in this chapter. Furthermore, it is only applicable under exposure to UV light which hinders the practical applicability of pure TiO$_2$ nanoparticles. Therefore, TiO$_2$-RGO nanohybrid is used

to address the above shortcomings. It is well-known that the TiO_2-RGO nanohybrid shows enhanced photocatalytic activity over pure TiO_2 nanoparticles and relatively small amount of RGO (up to 10–20 wt% with respect to TiO_2 nanoparticles) is effective for this enhancement.[41] Hence, sunlight induced photocatalytic degradation of MB solution led to a significant reduction in MB concentration when HPU/T_5RGO and HPU/T_{10}RGO nanocomposites were taken as photocatalysts. Whereas, pristine HPU and the HPU/T_1RGO nanocomposite did not show significant degradation efficiency. As TiO_2 nanoparticles are only responsible for degradation of the dye so the presence of a high amount of TiO_2 nanoparticles in the nanocomposite enhanced the dye degradation rate. Therefore, pristine HPU and the HPU/T_1RGO nanocomposite did not show effective dye degradation. During degradation, TiO_2-RGO nanohybrid presence in the nanocomposite absorbs the energy of sunlight and h^+/e^- pairs generated in TiO_2 nanoparticles. These photoexcited electrons then transferred to RGO sheet and react with the dissolved oxygen to form reactive oxygen species (ROS) as shown in **Scheme 6.1**. Also, photoexcited electrons presence on TiO_2 surface can also be trapped directly by the dissolved oxygen to form ROS such as $^.OH$ and $^.O_2^-$. The generated ROS react with water to form hydroxyl radicals as shown in **Scheme 6.1**. Then, organic pollutant (MB dye) is degraded by these hydroxyl radicals through chain reactions to decompose into small molecules. On the other side, holes generated in the valence band of TiO_2 react with absorbed water to form surface hydroxyl radicals which then degrade the pollutant to nontoxic compounds. Also, the generated holes can directly oxidize the dye molecules.[41]

A blank test without HPU or its nanocomposites was also performed and extremely slow degradation (only 10%) of the MB was found after 180 minutes of direct sunlight irradiation. Therefore, to achieve a sunlight induced self-cleaning HPU nanocomposite appropriate loading and compositional variation of the nanohybrid are crucial. The nanocomposite demonstrated significant dye degradability in the presence of sunlight. The HPU/T_{10}RGO10 nanocomposite efficiently degraded MB dye with 90 min of sunlight exposure with good reusability. The photocatalytic activity of the reused nanocomposite film was checked up to the third cycle as shown in **Figure 6.10**d. There is no significant decreased in dye degradability even after 3rd cycles. Therefore, it can be used as a surface coating material where it can remove the presence of organic dirt and provide a clean surface.
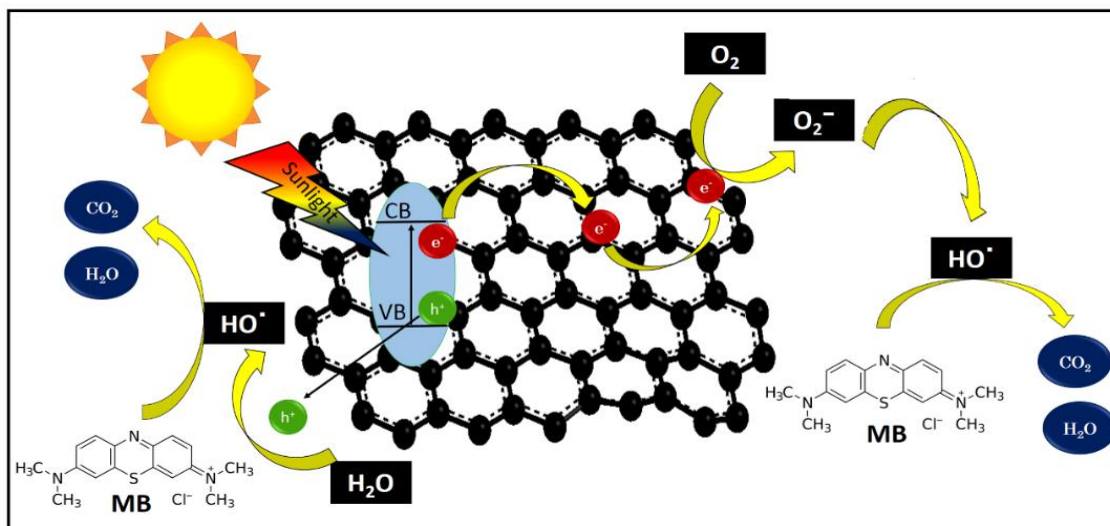
Scheme 6.1 Proposed mechanism of MB degradation

6.4. Conclusions

The study paved the way to prepare a tough elastomeric HPU/TiO₂-RGO nanocomposites at different loadings and compositions of the nanohybrid. The incorporation of nanohybrid in HPU matrix results improvements of thermal and mechanical properties such as tensile strength, tensile modulus, elongation at break and toughness. Interestingly, SME, self-healing and self-cleaning ability can be achieved by judicious choice of the composition and loading of the TiO₂-RGO nanohybrid in the nanocomposite. The simultaneous demonstration of such attractive properties by a single material widen the possible applications of the fabricated material in diverse advanced fields.

References

1. Liu, F., & Urban, M.W. Recent advances and challenges in designing stimuli-responsive polymers, *Prog. Polym. Sci.* **35**, 3--23, 2009.

2. Roy, D., et al. Future perspectives and recent advances in stimuli-responsive materials, *Prog. Polym. Sci.* **35**, 278--301, 2010.

3. Jochum, F.D., & Theato, P. Temperature- and light-responsive smart polymer materials, *Chem. Soc. Rev.* **42**, 7468--7483, 2013.

4. Lendlein, A., & Kelch, S. Shape-memory polymers, *Angew. Chem. Int. Ed.* **41**, 2034--2057, 2002.

5. Murphy, E.B., & Wudl, F. The world of smart healable materials, *Prog. Polym. Sci.* **35**, 223--251, 2010.

6. Bergman, S.D., & Wudl, F. Mendable polymers, *J. Mater. Chem.* **18**, 41--62, 2008.

7. Yang, Y., & Urban, M.W. Self-healing polymeric materials, *Chem. Soc. Rev.* **42**, 7446--7467, 2013.

8. Bedford, N.M., & Steckl, A.J. Photocatalytic self-cleaning textile fibers by coaxial electrospinning, *ACS Appl. Mater. Interfaces* **2**, 2448--2455, 2010.

9. Meng, H., & Li, G. A review of stimuli-responsive shape memory polymer composites, *Polymer* **54**, 2199--2221, 2013.

10. Habault, D., et al. Light-triggered self-healing and shape-memory polymers, *Chem. Soc. Rev.* **42**, 7244--7256, 2013.

11. Trask, R.S., & Bond, I.P. Biomimetic self-healing of advanced composite structures using hollow glass fibres, *Smart Mater. Struct.* **15**, 704--710, 2006.

12. Cho, S.H., et al. Self-healing polymer coatings, *Adv. Mater.* **21**, 645--649, 2009.

13. Toohey, K.S., et al. Self-healing materials with microvascular networks, *Nat. Mater.* **6**, 581--585, 2007.

14. Chen, X., et al. A thermally re-mendable cross-linked polymeric material, *Science* **295**, 1698--1702, 2002.

15. Chung, C.M., et al. Crack healing in polymeric materials via photochemical [2+2] cycloaddition, *Chem. Mater.* **16**, 3982--3984, 2004.

16. Charpentier, P.A., et al. Nano-TiO_2/polyurethane composites for antibacterial and self-cleaning coatings, *Nanotechnology* **23**, 425606 (pp 9), 2012.

17. Kalita, H., & Karak, N. Bio-based elastomeric hyperbranched polyurethanes for shape memory application, *Iran. Polym. J.* **21** (4), 263--271, 2012.

18. Binder, W.H. *Self-Healing Polymers: From Principles to Applications*, Willey-VCH, Germany, 2013.

19. Chin, P., & Ollis, D.F. Decolorization of organic dyes on Pilkington Activ™ photocatalytic glass, *Catal. Today* **123**, 177--188, 2007.

20. Nakata, K., et al. Antireflection and self-cleaning properties of a moth-eye-like surface coated with TiO_2 particles, *Langmuir* **27**, 3275--3278, 2011.

21. Dahl, M., et al. Titanium dioxide-based nanomaterials for photocatalytic, *Chem. Rev.* **114** (19), 9853--9889, 2014.

22. Akhavan, O., et al. Photodegradation of graphene oxide sheets by TiO_2 nanoparticles after a photocatalytic reduction, *J. Phys. Chem. C* **114**, 12955--12959, 2010,

23. Wang, W.S., et al. Large ultrathin anatase TiO_2 nanosheets with exposed {001} facets on graphene for enhanced visible light photocatalytic activity, *J. Phys. Chem. C* **116**, 19893--19901, 2012.

24. Bagheri, S., et al. Synthesis and characterization of anatase titanium dioxide nanoparticles using egg white solution via sol-gel method, *J. Chem.* **2013**, 848205 (pp 5), 2013.

25. Kuila, T., et al. A green approach for the reduction of graphene oxide by wild carrot root, *Carbon* **50** (3), 914--921, 2010.

26. Graf, D., et al. Spatially resolved Raman spectroscopy of single- and few-layer graphene, *Nano Lett.* **7**, 238--242, 2007.

27. Ferrari, A.C., & Robertson, J. Interpretation of Raman spectra of disordered and amorphous carbon, *Phys. Rev. B: Condens. Matter* **61**, 14095--14107, 2000.

28. Akhavan, O., et al. Adverse effects of graphene incorporated in TiO_2 photocatalyst on minuscule animals under solar light irradiation, *J. Mater. Chem.* **22**, 23260--23266, 2012.

29. Sher Shah, M.S.A., et al. Green synthesis of biphasic TiO_2-reduced graphene oxide nanocomposites with highly enhanced photocatalytic activity, *ACS Appl. Mater. Interfaces* **4**, 3893--3901, 2012.

30. Xu, Y.J., et al. New insight for enhanced photocatalytic activity of TiO_2 by doping carbon nanotubes: a case study on degradation of benzene and methyl orange, *J. Phys. Chem. C* **114**, 2669--2676, 2010.

31. Wang, P., et al. Synthesis of reduced graphene oxide-anatase TiO_2 nanocomposite and its improved photo-induced charge transfer properties, *Nanoscale* **3**, 1640--1645, 2011.

32. Sim, L.C., et al. Graphene oxide and Ag engulfed TiO$_2$ nanotube arrays for enhanced electron mobility and visible-light-driven photocatalytic performance, *J. Mater. Chem. A* **2**, 5315--5322, 2014.

33. Yadav, S.K., et al. Synthesis of mechanically robust antimicrobial nanocomposites by click coupling of hyperbranched polyurethane and carbon nanotubes, *Polymer* **53** (10), 2023--2031, 2012.

34. Yoo, H.J., et al. High-speed actuation and mechanical properties of graphene-incorporated shape memory polyurethane nanofibers, *J. Phys. Chem. C* **118**, 10408--10415, 2014.

35. Zheng, Y., et al. Hyperbranched polymers: Advances from synthesis to applications, *Chem. Soc. Rev.* **44**, 4091--4130, 2015.

36. Goncalves, G., et al. Graphene oxide modified with PMMA *via* ATRP as a reinforcement filler, *J. Mater. Chem.* **20**, 9927--9934, 2010.

37. Mauter, M.S., & Elimelech, M. Environmental applications of carbon-based nanomaterials, *Environ. Sci. Technol.* **42**, 5843--5859, 2008.

38. Bernardi, M., et al. Extraordinary sunlight absorption and one nanometer thick photovoltaics using two-dimensional monolayer materials, *Nano Lett.* **13** (8), 3664--3670, 2013.

39. Luo, X., & Mather, P.T. Shape memory assisted self-healing coating, *ACS Macro Lett.* **2** (2), 152--156, 2013.

40. Wang, C.C., et al. Rubber-like shape memory polymeric materials with repeatable thermal-assisted healing function, *Smart Mater. Struct.* **21**, 115010--115018, 2012.

41. Zhang, Y.H., et al. TiO$_2$−graphene nanocomposites for gas-phase photocatalytic degradation of volatile aromatic pollutant: Is TiO$_2$−graphene truly different from other TiO$_2$−carbon composite materials? *ACS Nano* **4**, 7303--7314, 2010.

42. Iliut, M., et al. Riboflavin enhanced fluorescence of highly reduced graphene oxide, *Chem. Phys. Lett.* **586**, 127--131, 2013.